

Cite this: *J. Mater. Chem. B*, 2022, 10, 3344

Construction of multifunctional cell aggregates in angiogenesis and osteogenesis through incorporating hVE-cad-Fc-modified PLGA/ β -TCP microparticles for enhancing bone regeneration

Linxue Zhang,^{†a} Zhuo Wan,^{†bc} Zuoying Yuan,^c Jun Yang,^{id d} Yunfan Zhang,^e Qing Cai,^{id *b} Jianyong Huang^{id *c} and Yuming Zhao^{*a}

Multicellular aggregates have been widely utilized for regenerative medicine; however, the heterogeneous structure and undesired bioactivity of cell-only aggregates hinder their clinical translation. In this study, we fabricated an innovative kind of microparticle-integrated cellular aggregate with multifunctional activities in angiogenesis and osteogenesis, by combining stem cells from human exfoliated deciduous teeth (SHEDs) and bioactive composite microparticles. The poly(lactide-co-glycolide) (PLGA)-based bioactive microparticles (PTV microparticles) were $\sim 15 \mu\text{m}$ in diameter, with dispersed β -tricalcium phosphate (β -TCP) nanoparticles and surface-modified vascular endothelialcadherin fusion protein (hVE-cad-Fc). After co-culturing with microparticles in U-bottomed culture plates, SHEDs could firmly attach to the microparticles with a homogeneous distribution. The PTV microparticle-integrated SHED aggregates (PTV/SHED aggregates) showed significant positive CD31 and ALP expression, as well as the significantly upregulated osteogenesis makers (Runx2, ALP, and OCN) and angiogenesis makers (Ang-1 and CD31), compared with PLGA, PLGA/ β -TCP (PT) and PLGA/hVE-cad-Fc (PV) microparticle-integrated SHED aggregates. Finally, in mice, 3 mm calvarial defects filled with the PTV microparticle-integrated SHED aggregates achieved abundant vascularized neo-bone regeneration within 4 weeks. Overall, we believe that these multifunctional PTV/SHED aggregates could be used as modules for bottom-up regenerative medicine, and provide a promising method for vascularized bone regeneration.

Received 17th February 2022,
Accepted 21st March 2022

DOI: 10.1039/d2tb00359g

rsc.li/materials-b

Introduction

Mesenchymal stem cell (MSC)-derived multicellular aggregates with a tissue-like structure formed under three-dimensional (3D) cell-culturing environments *ex vivo* have been widely used in drug screening, tissue engineering, and cell-based therapeutics.^{1,2} Compared with two-dimensional (2D) cell culture models, 3D culturing enables the formation of multicellular aggregates by creating more cell-to-cell and cell-to-extracellular matrix (ECM) interactions, thus significantly improving cell retention, paracrine signalling, and further tissue integration.^{3,4} For promoting bone repair, multicellular aggregates with an adequate MSC supplement and integration ability have shown great utility as implantable therapeutics.⁵ However, the self-assembly cell-only aggregates have intrinsic limitations in the transport of oxygen and nutrition, and show non-specific differentiation after transplantation, which may hinder their therapeutic efficacy and even cause repair failure.^{6–8}

Blood vessel infiltration provides an optimal microenvironment for nutrient and oxygen supply and removes metabolites,

^a Department of Pediatric Dentistry, Peking University School and Hospital of Stomatology & National Center of Stomatology & National Clinical Research Center for Oral Diseases & National Engineering Laboratory for Digital and Material Technology of Stomatology & Beijing Key Laboratory of Digital Stomatology & Research Center of Engineering and Technology for Computerized Dentistry Ministry of Health & NMPA Key Laboratory for Dental Materials, Beijing 100081, PR China. E-mail: yuming_zhao@hotmail.com

^b State Key Laboratory of Organic-Inorganic Composites & Beijing Laboratory of Biomedical Materials & Beijing University of Chemical Technology, Beijing 100029, PR China. E-mail: caiqing@mail.buct.edu.cn

^c Department of Mechanics and Engineering Science, College of Engineering, Peking University, Beijing 100871, PR China. E-mail: jyhuang@pku.edu.cn

^d The Key Laboratory of Bioactive Materials, Ministry of Education & College of Life Science, Nankai University, Tianjin 300071, PR China

^e Department of Orthodontics, Peking University School and Hospital of Stomatology & National Center of Stomatology & National Clinical Research Center for Oral Diseases & National Engineering Laboratory for Digital and Material Technology of Stomatology & Beijing Key Laboratory of Digital Stomatology & Research Center of Engineering and Technology for Computerized Dentistry Ministry of Health & NMPA Key Laboratory for Dental Materials, Beijing 100081, PR China

[†] These authors contributed equally to this work.

hence promoting the viability of MSC aggregates.⁹ During the process of bone-tissue regeneration, sufficient angiogenesis facilitates cell proliferation and tissue ingrowth; by contrast, scarce vascular infiltration leads to tissue central necrosis, osseointegration failure and fibrous encapsulation.^{10–12} Although the porous structure between stacked aggregates allows the vessels to grow in, the absence of inducing factors make these self-assembly cell-only aggregates difficult to rebuild the complex architecture of natural tissue, especially the vascular networks.¹³

Vascular endothelial cadherin fusion protein (hVE-cad-Fc) is a fusion protein that consists of the extracellular domain of human VE-cadherin and the Fc region of immunoglobulin IgG.¹⁴ hVE-cad-Fc has inherited partial characteristics of vascular endothelial-cadherin (VE-cadherin) which plays a pivotal role in vascular remodelling.^{15–17} It has been reported that the hVE-cad-Fc matrix can trigger the intracellular signals (VEGFR2/FAK-AKT/PI3K) and promotes the endothelial differentiation of hMSCs *in vitro*.¹⁸ In our previous work, poly(lactide-co-glycolide) (PLGA) scaffolds modified by hVE-cad-Fc have been demonstrated to promote the adhesion, proliferation, secretion, endothelial differentiation of hMSCs, and achieve vascularization *in vivo*.¹⁹ It is a feasible strategy to introduce hVE-cad-Fc to induce vascularization in multicellular aggregates based therapeutics.

In addition, the dense cell-accumulation structure often hinders the diffusion of oxygen and nutrition inside the multicellular aggregates, hence forming anoxic necrotic cores.²⁰ The integration of microscaffolds into MSC aggregates has been shown to be a promising method to improve the viability of inner cells.^{21–23} In particular, the bioactive ingredients that are encapsulated in the microscaffolds can drive cells to directionally differentiate to a specific phenotype.^{24–27} Calcium phosphate compounds, such as hydroxyapatite (HAP) have been widely used as osteogenic inducer. For example, it has been reported that HAP-coated microparticles significantly stimulates osteogenic markers that are up-regulating in the multicellular aggregates of murine embryonic stem cells (ESCs).^{28,29} However, the high crystallinity makes HAP quite difficult to dissolve and/or degrade under physiological conditions.³⁰ β -Tricalcium phosphate (β -TCP), which displays a high similarity in structure and solubility to bone mineral, is easy to be replaced by new bone, and has emerged as one of the most attractive bone-graft materials that can be used instead of hydroxyapatite.^{31,32}

In this study, we designed an innovative type of composite microparticle-integrated cellular aggregate with multifunctional activities in angiogenesis and osteogenesis. A two-stage emulsion method was designed to fabricate microparticles composed of poly(lactide-co-glycolide) (PLGA) and β -TCP (PT microparticles). Subsequently, hVE-cad-Fc was immobilized on the surface of PT microparticles to obtain bioactive PTV microparticles. Stem cells from human exfoliated deciduous teeth (SHEDs), a type of stem cells originating from the neural crest with non-immunogenicity and a higher proliferative potential than traditionally used dental pulp stem cells (DPSCs),^{33,34} were

co-cultured with PTV microparticles in round-bottomed (U-bottomed) culture plates to fabricate multifunctional microparticle-integrated SHED aggregates (PTV/SHED aggregates). The composite aggregates with SHEDs and modified microparticles are able to mimic the bone-tissue-like structure *ex vivo* and induce vascularized bone regeneration *in vivo*.

Experimental

Material

PLGA (lactide : glycolide = 75 : 25, MW = 50 000) was purchased from Shandong Pharmaceutical Sciences Pilot Plant (China), β -TCP (particle size \sim 10 nm) was provided by Institute of Metal Research, Chinese Academy of Sciences, hVE-cadherin-Fc was provided by the laboratory of Yang Jun, Nankai University, and all other reagents/solvents were purchased from Aladdin (China).

Preparation and characterization of PLGA/ β -TCP microparticles

PLGA/ β -TCP (PT) microparticles were produced using a two-stage emulsion method. Briefly, PLGA (1 g) and Span 80 (0.1% w/v) were dissolved in dichloromethane (DCM; 20 mL), then β -TCP (200 mg) was added to the PLGA/DCM solution through homogenization (15 000 rpm) to form the first stage of the emulsion, which is a solid-in-oil (S/O) phase. Then the S/O phase was added to 10 mL of poly(vinyl alcohol) (PVA) aqueous solution (1% w/v) containing Tween 60 (0.1% w/v) and dispersed using a homogenizer (IKA Germany) to form the second stage of emulsion, which is a solid-in-oil-in-water (S/O/W) phase. Finally, the suspension was added dropwise into 200 mL of poly(vinyl alcohol) (PVA) aqueous solution (1% w/v) containing Tween 60 (0.1% w/v), and the system was continuously stirred (500 rpm) for 6 h at room temperature to allow solvent evaporation. The solidified microparticles were collected, washed with deionized water, and lyophilized. The morphology of the prepared microparticles was observed and imaged using a scanning electron microscope (SEM; JEOL JSM-7500F, Japan). Elemental mapping and energy dispersive spectroscopy (EDS) analysis was performed using the same parameters as for SEM observations.

Modification of PLGA and PLGA/ β -TCP microparticles with hVE-cad-Fc

To modify the PLGA and PLGA/ β -TCP microparticles with hVE-cad-Fc, microparticles were dispersed in the hVE-cad-Fc/PBS solution (w/v%) and incubated at 37 °C with continuous stirring (100 rpm) for 2 h and collected *via* centrifugation at 12 000 rpm at 4 °C for 5 min.

VE-cadherin immunofluorescence staining was performed to visualize the bound hVE-cad-Fc on the PLGA and PLGA/ β -TCP microparticles. In brief, hVE-cad-PLGA (PV) and hVE-cad-PLGA/ β -TCP (PTV) microparticles were blocked using a 5% BSA/PBS solution for 1 h and treated with goat anti-human IgG (1 : 50, Solarbio, Beijing, China). Fluorescence images were obtained using a CLSM (Leica, Wetzlar, Germany) and analysed quantitatively using software ImageJ software (version 1.47,

National Institutes of Health, USA). Unmodified microparticles were used as a control.

Cell culture

Normal stem cells from exfoliated human deciduous teeth were derived from the Oral Stem Cell Bank (China, Beijing). The cells were cultured in α -modified Eagle medium (α -MEM; Gibco, USA) supplemented with 10% fetal bovine serum (FBS; Gibco, USA), 100 IU mL⁻¹ penicillin (Sigma, USA) and 100 mg mL⁻¹ streptomycin (Sigma, USA). The culture system was maintained at 37 °C under saturated humidity supplied with 5% CO₂. For osteogenic differentiation testing, the osteogenic differentiation medium was made by adding 0.05 mmol L⁻¹ vitamin C (Sigma, USA), 10 mmol L⁻¹ α -sodium glycerophosphate (Sigma, USA) and 1 × 10⁻⁸ mol L⁻¹ dexamethasone (Sigma, USA) to the culture medium. The medium was refreshed every 2 days in all the cell-culture cases. For the cell culture with microparticles, before seeding the cells, microparticles were irradiated with ultraviolet light for 2 h.

Adhesion and proliferation test

For evaluation of adhesion and proliferation, 2000 SHED cells per well were seeded on a 96-well culture plate with various microparticles (PLGA ± β -TCP ± hVE-cad-Fc) for 4 hours, or 1, 3 and 5 days, with tissue culture polystyrene (TCP) used as the control. The cell adhesion and proliferation were evaluated using a Cell Counting Kit-8 (CCK-8; Dojindo, Japan) assay.

In vitro osteogenic differentiation test

A Transwell system was prepared for the evaluation of osteogenic differentiation. 0.1 mg various microparticles were placed on the Transwell inserts and SHEDs were seeded in 24-well plates at a density of 10 000 cells per well and randomly divided into five groups: (1) TCP group (cultured with induction medium), (2) PLGA group, (3) PLGA + β -TCP (PT) group, (4) PLGA + VE-cad (PV) group, (5) PLGA + β -TCP + VE-cad (PTV) group. After culturing, the cells were rinsed with phosphate-buffered saline (PBS) and fixed in 4% paraformaldehyde for further analysis. For ALP staining, the treated cells were stained using the ALP color development kit (Beyotime, China) after 7 days of culturing. For Alizarin Red S (ARS) staining, the treated cells were soaked in Alizarin Red S working solution (1%, w/v) after 14 days of culturing. The staining images were qualified using ImageJ software (version 1.47, National Institutes of Health, USA).

Chicken embryo allantoic membrane (CAM) model for angiogenesis assay

Fertilized chicken embryos were incubated at 38.3 °C under 60% humidity for 5 days. Then, a 4 mm-diameter round window was created on the eggshell and the shell membranes were removed to expose the CAM. 200 μ L of PBS containing 0.1 mg of various microparticles was pipetted onto the CAM, and the treated chicken embryos were incubated at 38.5 °C under 60% humidity for another 5 days. PBS without microparticles was used as the control. Finally, the CAMs were

collected and fixed using buffered formalin for 1 h. Then the CAMs were visualized using a stereomicroscope (PXS6-T, CeWei, China). Neovascular blood vessel branches, junctions and end points were analyzed using AngioQuant software (Version 1.33, Mathwork Inc, Houston, TX, USA).

Preparation and characterization of SHED aggregates integrated with microparticles

To prepare SHED aggregates integrated with microparticles, cell suspension with a density of 30 000 cells mL⁻¹ was prepared and various microparticles were mixed with the cell suspension at the ratio of 1 : 3. Then the mixed suspension of cells and microparticles (0.2 mL well⁻¹) was added into 96-well round-bottomed (U-bottomed) culture plates. The plates were centrifuged at a speed of 1000 rpm for 5 min to reunite the cells and microparticles, then the plates were incubated at 37 °C. After 24 h, the cell aggregates that formed were observed and imaged using an optical microscope (Olympus, Tokyo, Japan). SHED aggregates without microparticles were also prepared and used as controls.

Viability and biological functions of SHEDs in aggregates

Live/dead staining was performed to examine the vitality of the cell aggregates. At day 1, the samples were treated with a calcein-AM/PI double-stain kit (Solarbio, China) and the fluorescence images were captured *via* CLSM. Dead cells showed red fluorescence, and live cells showed green fluorescence.

For RT-PCR assays, after 7 or 14 days of osteogenic induction, the cell aggregates were rinsed with PBS and isolated using Trizol reagent (Ambion[®], Life Technologies[™], USA) to extract the total RNA. The quality and approximate concentration of RNA was determined using a NanoDrop 8000 spectrophotometer (Nanodrop Technologies, Wilmington, DE, USA). Then, cDNA was reverse-transcribed using the PrimeScript[®] RT reagent Kit (Takara, Japan) according to the manufacturer's protocol. RT-PCR was performed using SYBR Green Master (Roche, USA). GAPDH served as a housekeeping gene for normalization of the data. The specific primers of two angiogenic-related genes and three osteogenic-related genes, including those encoding CD31, Ang-1, Runx2, ALP, and OCN, were designed as listed in Table 1.

Table 1 Primer sequences for RT-PCR

Gene	Primer sequences
GAPDH	Forward: 5'-GGA GCG AGA TCC CTC CAA AAT-3' Reverse: 5'-GGC TGT TGT CAT ACT TCT CAT GG-3'
RUNX2	Forward: 5'-ACT ACC AGC CAC CGA GAC CA-3' Reverse: 5'-ACT GCT TGC AGC CTT AAA TGA CTC T-3'
ALP	Forward: 5'-ATG GGA TGG GTG TCT CCA CA-3' Reverse: 5'-CCA CGA AGG GGA ACT TGT C-3'
OCN	Forward: 5'-CAC TCC TCG CCC TAT TGG C-3' Reverse: 5'-CCC TCC TGC TTG GAC ACA AAG-3'
ANG-1	Forward: 5'-AGC ACT ATG ATG CCA AAC C-3' Reverse: 5'-CAA GTG GTG ACC TGG AAA G-3'
CD31	Forward: 5'-GTG AGG GTC AAC TGT TCT GT-3' Reverse: 5'-GTG ACC AGT TCA CTC TTG GT-3'

Hematoxylin and eosin (H&E) and immunohistochemical (IHC) staining (including ALP and CD31) were evaluated to further reveal the morphologies and biological functions of the aggregates. After 7 days of culturing under an osteogenic differentiation medium, the samples were collected and dehydrated using ethanol *via* a gradient method, then embedded in paraffin for histological section slicing.

Critical-sized calvarial defect model

A calvarial defect model in BALB/c nude mice was used to visualize the osteogenic regenerative capacity of the different groups. All experimental animal procedures were approved by the Animal Care and Use Committee of Peking University (China) in accordance with international standards on animal welfare (authorization number: LA2021529). For the animal surgery, 6–8-week-old BALB/c nude mice (Weitonglihua Biotechnology, Beijing, China) were anaesthetized *via* intraperitoneal injection of 1% pentobarbitone (8 mL kg⁻¹). After the nude mice were anaesthetized, a full-thickness defect 3 mm in diameter was created in the central region of the cranial bone using a dental surgical bur. The mice were randomly divided into three groups for implantation: ① blank group ($n = 4$), where the defects were left unfilled; ② PLGA group ($n = 4$), where the defects were filled with the PLGA/SHED aggregates; and ③ PTV group ($n = 4$), where the defects were filled with the PTV/SHEDs aggregates. After surgery, all the mice were allowed to move freely with food and water provided *ad libitum*. The animals were sacrificed at 4 weeks by injecting a lethal dose of the anesthetic drug into the abdominal cavity. Harvested samples were fixed for at least 24 h for further imaging and histological analysis.

Characterization of vascularized bone regeneration

The cranial bone specimens were scanned using an Invest MM Gantry-Std CT system (Siemens, Munich, Germany) at 80 kV and 500 μ A. The bone volume/total volume (BV/TV) ratio was calculated using Inveon Research Workplace 3.0 software (Siemens). After micro-CT analysis, the fixed specimens were decalcified in 10% ethylenediaminetetraacetic acid (EDTA) for 7 days, followed by dehydration and embedding in paraffin for histological section slicing. Sections were cut into 4-mm-thick slices and stained using hematoxylin and eosin (H&E), Masson's trichrome staining (Solarbio, Beijing, China) and immunohistochemical staining of CD31. All histological sections were observed using a light microscope.

Statistical analysis

All the data were analyzed using SPSS 24.0 software (IBM Corp, Armonk, NY, USA) and expressed as the mean \pm standard deviation (SD). Unpaired Student's *t*-tests and one-way analysis of variance (ANOVA) were applied for the statistical analysis. Differences between various groups with $*P < 0.05$ were considered statistically significant and $**P < 0.01$ was considered highly significant.

Results and discussion

Fabrication and characterizations of hVE-cad-Fc-modified PLGA/ β -TCP microparticles

A schematic illustration of the fabrication of the PT microparticles is shown in Fig. 1A. The microparticles were fabricated using an (S/O)/W/W two-stage emulsion method. β -TCP nanoparticles (the solid phase) were dispersed into PLGA solution (the oil phase), and then the (S/O) mixed phase was dispersed in PVA solution to form microparticles under continuous stirring. Finally, the preformed microparticles were added dropwise in large amounts of PVA solution for further solvent evaporation and structure formation. For comparison, PLGA microparticles without any additive were also prepared.

The morphologies of the microparticles were observed *via* SEM. As shown in Fig. 1B, the average diameters of all the microparticles were controlled to be around 15 μ m on average, which was similar to the size of the SHEDs. It has been reported that the microparticle size can influence the fabrication and functional induction of aggregates.³⁵ Microparticles smaller than 2 μ m often exhibit significant cell internalization and in general are localized in the perinuclear region, which has no significant influence on the cell aggregate structures.³⁶ In addition, large microparticles with diameters over 50 μ m always play the role of a cell-carrier instead of constituting the cell aggregate due to their lower surface area to volume ratios.³⁷ Hence, cell-sized microparticles are considered to be an appropriate choice for cell aggregate culturing.^{38–40}

The PT microparticles displayed rough surfaces due to the incorporation of β -TCP nanoparticles, which were homogeneously scattered on the surface. By contrast, the PLGA microparticles showed a smooth surface. EDS mapping was employed to investigate the elemental composition. The existence of β -TCP in the PT microparticles was assessed *via* the intense calcium (red) signals and phosphorus (blue) signals (Fig. 1C). In addition, as confirmed through TGA analysis, the residual weight detected for PT microparticles was 17.17%, whereas the residual weight for PLGA microparticles was only 0.27% (Fig. 1D). Both of these results confirmed that β -TCP had been successfully blended into the PT microparticles. FTIR revealed the presence and state of the components in the microparticles (Fig. 1E). The characteristic peaks around 1750 cm⁻¹ (C=O group), and 1260 cm⁻¹ (C–O–C group) are attributed to PLGA.⁴¹ In the PT microparticles, the peak at 640 cm⁻¹ represented the presence of β -TCP. These results demonstrated that the addition of β -TCP had no adverse effect on the molecular structure of PLGA.

hVE-cad-Fc is a fusion protein consisting of the human vascular endothelial-cadherin extracellular domain and the immunoglobulin IgG Fc region.⁴² The Fc domain of IgG can bind with the surface of biomaterials *via* hydrophobic interactions.⁴³ In our previous work, hVE-cad-Fc was used as an artificial matrix on polystyrene plates for human umbilical vein endothelial cells (HUVECs).⁴² To modify the microparticles with hVE-cad-Fc in this work, PLGA or PT microparticles were soaked in hVE-cad-Fc solution and stirred for 2 hours (Fig. 2A). IgG immunofluorescence was used to detect the presence of

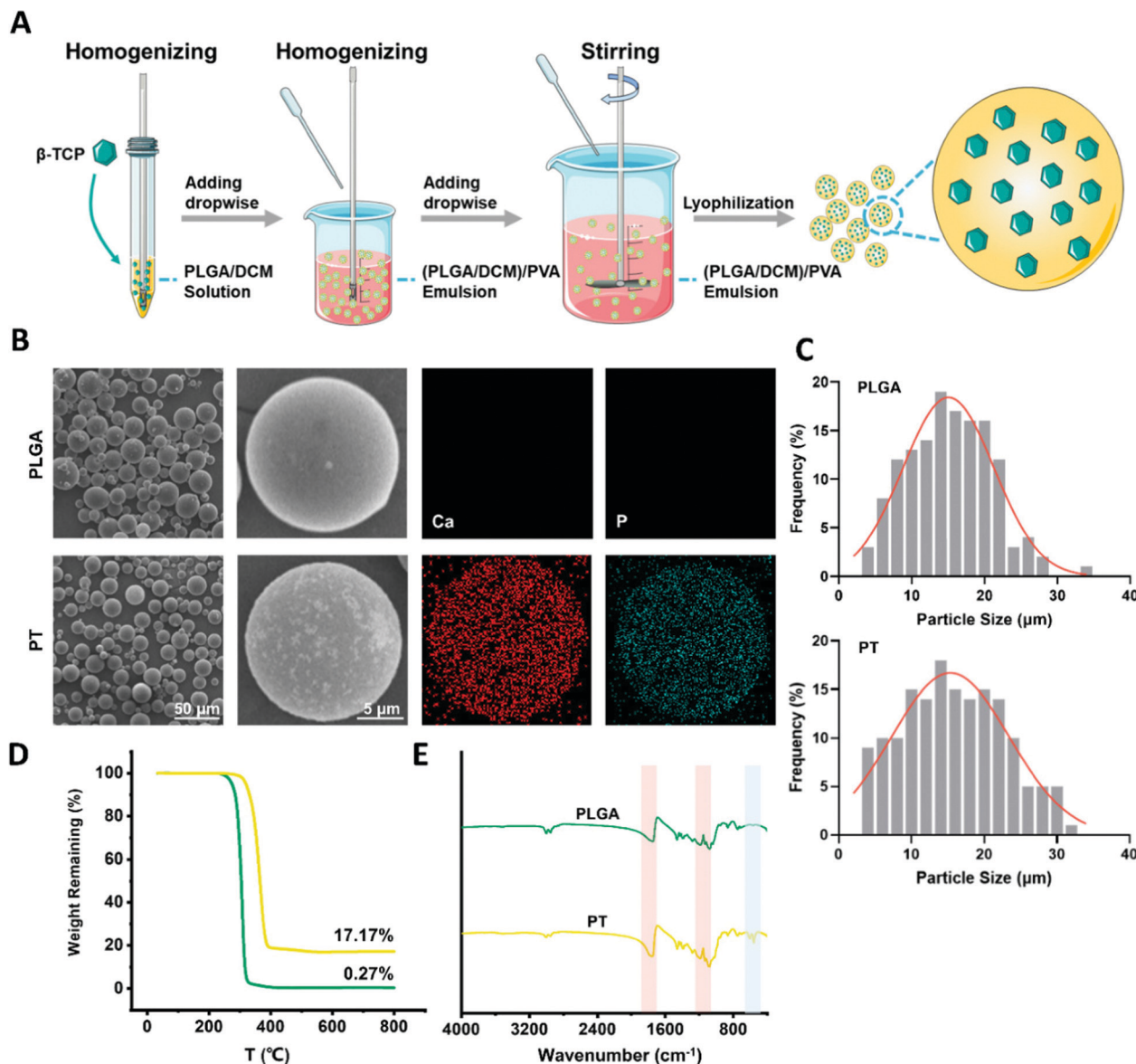


Fig. 1 Fabrication and characterization of the microparticles. (A) Schematic illustration showing the fabrication process for PLGA microparticles and PLGA/ β -TCP microparticles. (B) SEM images showing the morphology and the elemental distribution of various microparticles. (C) Size distribution of the various microparticles. (D) TGA curves and (E) FTIR spectra of the microparticles with and without embedding of β -TCP nanoparticles.

hVE-cad-Fc. As shown in Fig. 2B, the even green fluorescence signals could be seen on the surface of the hVE-cad-Fc-modified microparticles, while no signal was detected on the PLGA and PT groups, indicating that hVE-cad-Fc was uniformly immobilized on the surfaces of the microparticles. Quantitative of fluorescence staining showed that the PT microparticles have a stronger adsorption capacity for hVE-cad-Fc than the PLGA microparticles (Fig. 2C), which might be due to the rough surface caused by the addition of β -TCP.

Adhesion and proliferation of SHEDs cultured with microparticles

Cell adhesion is a prerequisite for subsequent cell survival and proliferation in 3D cell culture and cellular aggregate formation,

which represents the adaptation of a cell to its micro-environment.⁴⁴ As determined using a 4 hour CCK8 test, the groups with hVE-cad-Fc showed a significant improvement for the adhesion of cells (Fig. 3A). After 5 days of culturing, no apparent difference was found between the cells grown with microparticles, indicating that the compounded microparticles did not influence the cell growth, and the high biocompatibility of the materials was confirmed (Fig. 3B).

Osteogenic differentiation of SHEDs cultured with microparticles

SHEDs are a unique type of MSCs, which are derived from the pulp of the deciduous teeth and have been identified as being capable of differentiating into a variety of cell types, including

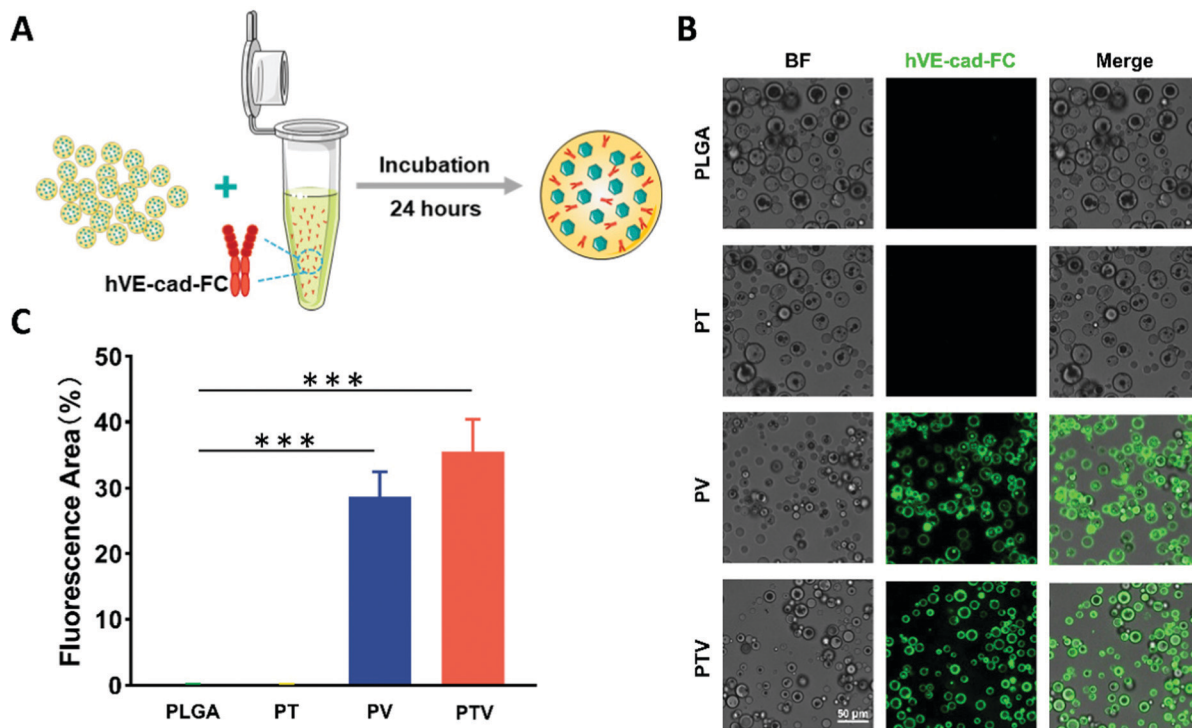


Fig. 2 Characterization of hVE-cad-Fc-modified microparticles. (A) Schematic illustration showing the modification process for hVE-cad-Fc/PLGA microparticles (PV) and hVE-cad-Fc/PLGA/ β -TCP microparticles (PTV). (B) Fluorescent and merged phase/fluorescent images of PLGA, PT, PV and PTV microparticles. (C) Semi-quantification of various microparticles via fluorescence staining ($*p < 0.05$, $**p < 0.01$, $***p < 0.001$).

neural cells, odontogenic cells, adipocytes, and osteoblasts.⁴⁵ Compared with human bone marrow mesenchymal stem cells (hBMSCs) and human dental pulp stem cells (hDPSCs), which are widely used in bone-tissue engineering, SHEDs possess a higher paracrine function for bone regeneration.⁴⁶ To investigate the effect of various microparticles on the osteogenic differentiation of SHEDs, the Transwell system was prepared (Fig. 3C). The expressions of ALP and calcium deposits, which are representative markers of the initial and terminal stages of osteogenesis, were evaluated. As shown in Fig. 3D and E, there was a much deeper staining color that could be observed in the PT and PTV groups compared with the other groups at day 7, which represented an obvious increase in ALP production. In addition, ARS staining also showed that the PTV group produced distinctly more mineral deposits after continuous osteogenic induction for 14 days, followed by the PT group (Fig. 3D and F). These results suggested that the microparticles with the addition of β -TCP exhibited a higher osteogenic ability than the other groups, and the combination of β -TCP and hVE-cad-Fc showed a synergetic effect, hence highly promoting osteogenesis. It is reasonable to assume that the PTV microparticles might have the potential to promote osteogenesis after integrated in the SHED aggregates.

Pro-angiogenic potential of microparticles

In addition to promoting cell adhesion, hVE-cad-Fc has also showed a capacity for reconstruction of the pro-vascularization microenvironment.⁴⁷ As reported in previous studies, hVE-cad-Fc-modified hydrogels and an hVE-cad-Fc-immobilized PLGA

scaffold showed enhanced vascularization both *in vitro* and *in vivo*.^{18,48} Here, to further explore the effect of microparticles on angiogenesis, a chicken embryo allantoic membrane (CAM) test was performed, as shown in Fig. 4A. For this, 0.1 mg various microparticles dispersed in PBS were placed on the surface of the chicken embryo allantoic membrane. After incubation for 5 days, the neo-vessel formation was imaged and analyzed. The total number of end points, the total vessel length and the total number of junctions formed at 5 days post-injection were observed in the interesting zones, and represented the capacity of angiogenesis. As shown in Fig. 4B–E, the PTV group and the PV group exhibited a significantly higher level of neovascular formation with the highest total number of end points, junctions, and total vessel length, and there was no significant difference between the PTV group and the PV group. These results confirmed that the hVE-cad-modified microparticles remarkably improved the angiogenesis potential, while PLGA and PT microparticles showed almost no improvement in vascular formation.

Viability of microparticle-integrated SHED aggregates

Taking cell adhesion, osteogenic differentiation, and pro-angiogenic potential together, it was proposed that the PTV microparticles would be more efficient in forming SHED aggregates with multifunctional activities in angiogenesis and osteogenesis. In this work, various aggregates were fabricated by mixing 6000 cells per well for the SHEDs and 2000 particles per well of the different microparticles after centrifugation; the

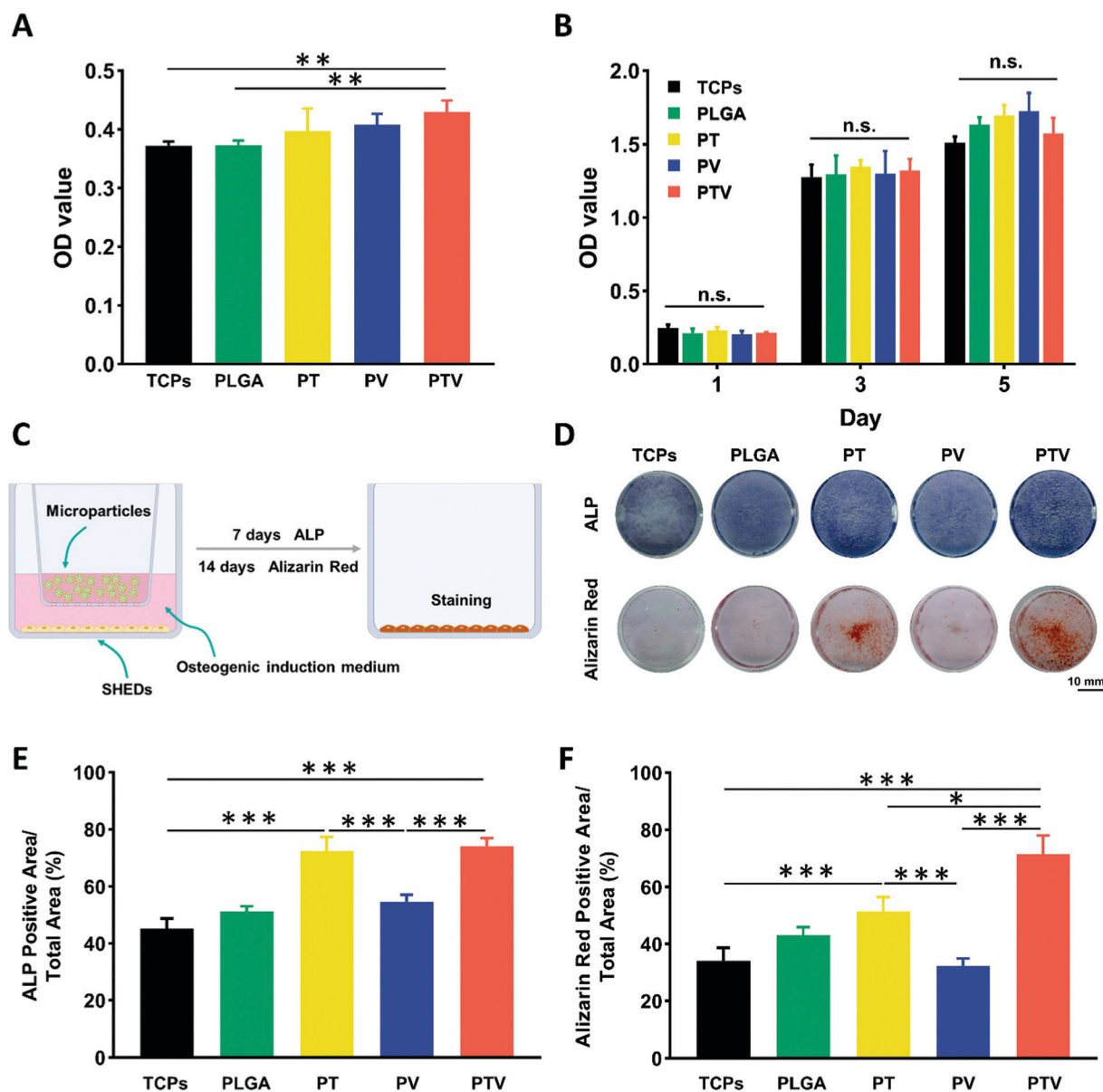


Fig. 3 Adhesion, proliferation and osteogenic differentiation of SHEDs cultured with microparticles. (A) Adhesion was quantitatively evaluated at 4 hours via CCK8 test. (B) Proliferation was quantitatively evaluated at days 1, 3, and 5 via CCK8 test. (C) Schematic illustration showing the Transwell system used for culturing of the SHEDs. (D) ALP staining was conducted for cells at day 7, and ARS staining was conducted for cells at day 14, and (E and F) semi-quantitative analysis of ALP and ARS staining ($p < 0.05$, $**p < 0.01$, $***p < 0.001$).

microparticle-free group was also prepared as a blank control (Fig. 5A). These aggregates were carefully harvested for further staining and analysis.

Cell necrosis in the aggregate core has been a major challenge for maintaining the viability of cellular aggregates, and cell necrosis inside the aggregates will be enhanced as the density of the seeding cells or the culture time is increased.⁴⁹ However, with the integration of microscaffolds in aggregates, the viability of the inner cells will be significantly improved.⁵⁰ After 1 day of culturing, live/dead staining was used to illustrate the cell viability and morphology of the cell aggregates. As shown in Fig. 5B, cell-only aggregates showed clear red fluorescence signals, which represented dead cells. Conversely, the

microparticle-integrated SHED aggregates showed a negligible number of dead cells with no significant difference among these groups, indicating that the incorporation of microparticles effectively improved cell viability in the aggregates. As shown by the H&E staining (Fig. 5C), the microparticle-integrated SHED aggregates presented as compacted spheroids with the microparticles distributed evenly throughout the whole region. After 7 days of culturing, the diameter of cell-only aggregates was about 95.2 μm . With the addition of microparticles, the average diameter of the aggregates was 131.3 μm (PLGA), 137.3 μm (PT), 135.0 μm (PV), 154.2 μm (PTV), respectively, which was a significant difference compared with the cell-only aggregates.

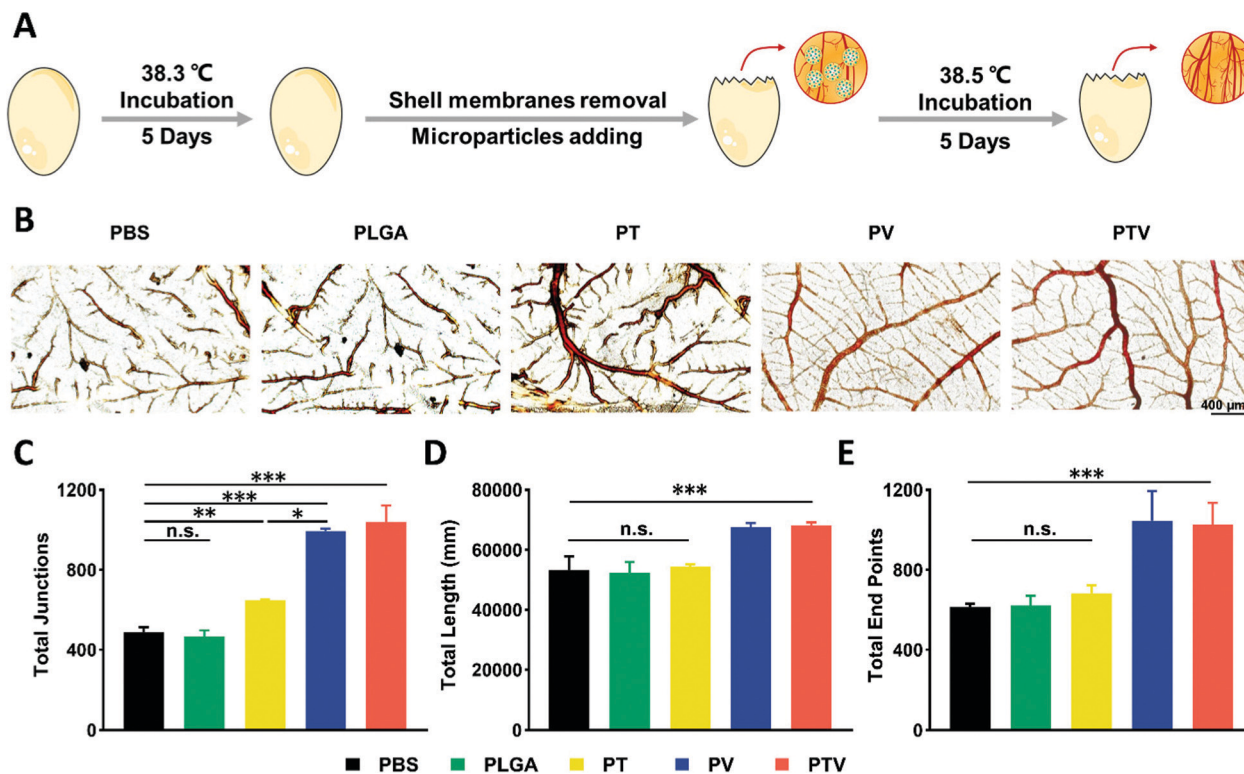


Fig. 4 Pro-angiogenic potential of microparticles. (A) Schematic illustration showing the process for various microparticles added to the CAM to test the angiogenic capacity compared with the control group (the addition of PBS). (B) Representative images of the various groups presented after 5 days of incubation, and the angiogenic capacity of the different groups was quantified via total tubular junctions (C), lengths (D) and end points (E) (* $p < 0.05$, ** $p < 0.01$, *** $p < 0.001$).

Osteogenesis and angiogenesis function of microparticle-integrated SHED aggregates

In order to evaluate the osteogenesis and angiogenesis function of these SHEDs aggregates, IHC staining and RT-qPCR was performed (Fig. 5A). After 7 days of culturing, the IHC staining of ALP confirmed the induction of osteogenesis in the β -TCP-containing microparticle-integrated SHED aggregate groups. Both PT and PTV groups exhibited positive dark-brown staining (Fig. 6A), and the quantitative results for ALP expression in the PT and PTV groups were over 2-fold than the β -TCP-free groups (SHEDs only, PLGA, and PV) (Fig. 6B). In addition, the expressions of osteogenesis markers (e.g., Runx2, ALP, and OCN) were evaluated using RT-qPCR (Fig. 6C). For the osteogenesis-related genes of the early stage, the mRNA levels of Runx2 in the PT and PTV group showed an over 3-fold upregulation at day 7 compared with the other β -TCP-free groups, and no significant difference was shown between the groups at day 14. In addition, ALP and OCN as the osteogenesis-related genes of middle and terminal stages, mRNA expression in the PT and PTV groups were also promoted at days 7 and 14 compared with the other groups. These results demonstrated that groups with coordinated β -TCP showed significant potential for osteogenesis compared with the SHEDs-only or β -TCP-free groups.

We further analyzed the angiogenesis potential of various SHED aggregates. The PV group and the PTV group showed clear staining of CD31 via IHC at day 7, while the positive

staining area was negligible for groups with the absence of hVE-cad (Fig. 6D). Quantitative analysis of the CD31 positive area (Fig. 6E) was in accordance with the gene expression of angiogenesis markers Ang-1 and CD31 (Fig. 6F), and the highest expressions were achieved in the PTV group, which was 1.76-fold and 1.78-fold higher than the SHEDs-only group, respectively. These results indicated that the hVE-cad-functionalized microparticles had the ability to promote *ex vivo* angiogenesis of SHEDs.

PTV microparticle-integrated SHED aggregates promote vascularized bone regeneration *in vivo*

All the *ex vivo* results confirmed that the PTV microparticle-integrated SHED aggregates, which contained both β -TCP and hVE-cad, showed desirable multifunctional activities in angiogenesis and osteogenesis. Hence, PTV microparticle-integrated SHED aggregates were selected for *in vivo* studies, and we speculated that such multifunctional aggregates had the potential to regenerate vascularized bone in critical sized bone defects. In addition, the PLGA microparticle-integrated SHED aggregates (PLGA), which were presented as non-functional aggregates, were utilized as the control group.

We established an orthotopic cranial bone defect model to examine the vascularized bone regeneration ability of PTV microparticle-integrated SHED aggregates *in vivo*. To avoid SHED aggregates being eliminated by the mouse immune

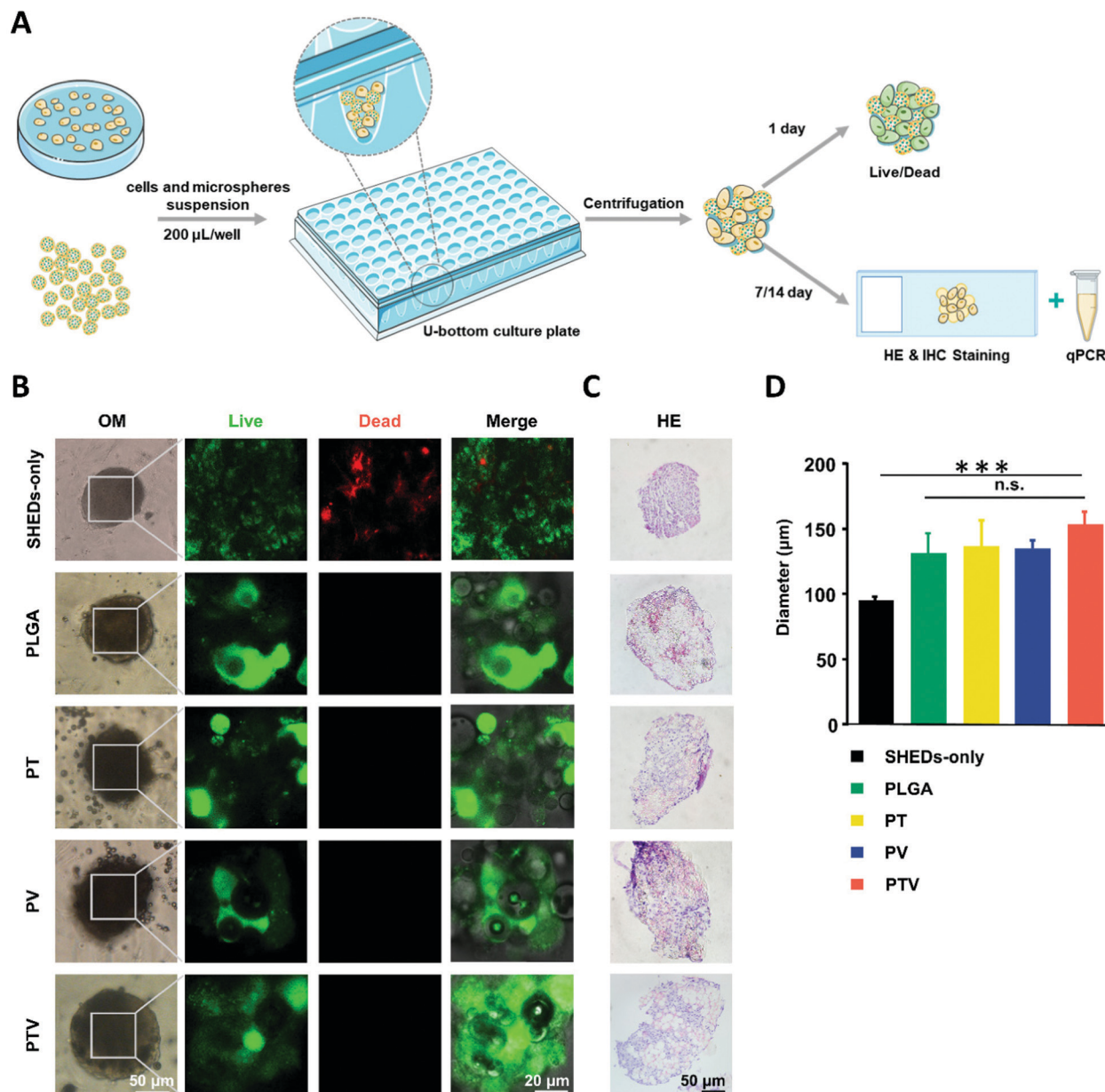


Fig. 5 Characterization and viability of microparticle-integrated aggregates. (A) Schematic representation of the construction of SHED aggregates integrated with microparticles. (B and C) Cell viability and morphology of the cell aggregates observed using an optical microscope (OM), live/dead staining (B) and H&E staining. (D) Diameter of SHED aggregates ($*p < 0.05$, $**p < 0.01$, $***p < 0.001$).

system after implantation, BALB/c nude mice with cell-mediated immunologic deficiencies were used for the experiments.⁵¹ For mice, 3-mm-diameter full-thickness calvarial defects have been widely used for bone regeneration studies,^{52–54} and it has been reported that 3 mm full-thickness calvarial bone shows no spontaneous healing within 8 weeks,⁵⁵ and thus can be considered as a critical bone defect. After implantation for 4 weeks, the micro-CT images were reconstructed and analyzed to evaluate the 3D structure and amount of new bone regenerated in the bone defect model (Fig. 7A). At 4 weeks post-operation, few neo-bone tissues had formed in the PLGA group as well as in the blank group. Conversely, the defects filled with PTV groups showed the clear

formation of new bone tissue sprouting from the defect edge, and clear formation of a bony bridge extending to the center of the defect (Fig. 7B). In particular, the neo-bone tissue in the central part of the defect area of the PTV group reached new bone volume/total volume (BV/TV) fraction values of 12.46% (Fig. 7C).

Histological analysis was performed to verify the maturity of the newly formed bone tissue and vascular remodeling. As shown in Fig. 7D, H&E staining showed that the implantation of various aggregates caused no obvious inflammatory response in the defect area, indicating that these aggregates had excellent biocompatibility. The defect areas in the blank and PLGA groups were mainly filled with fibrous tissue,

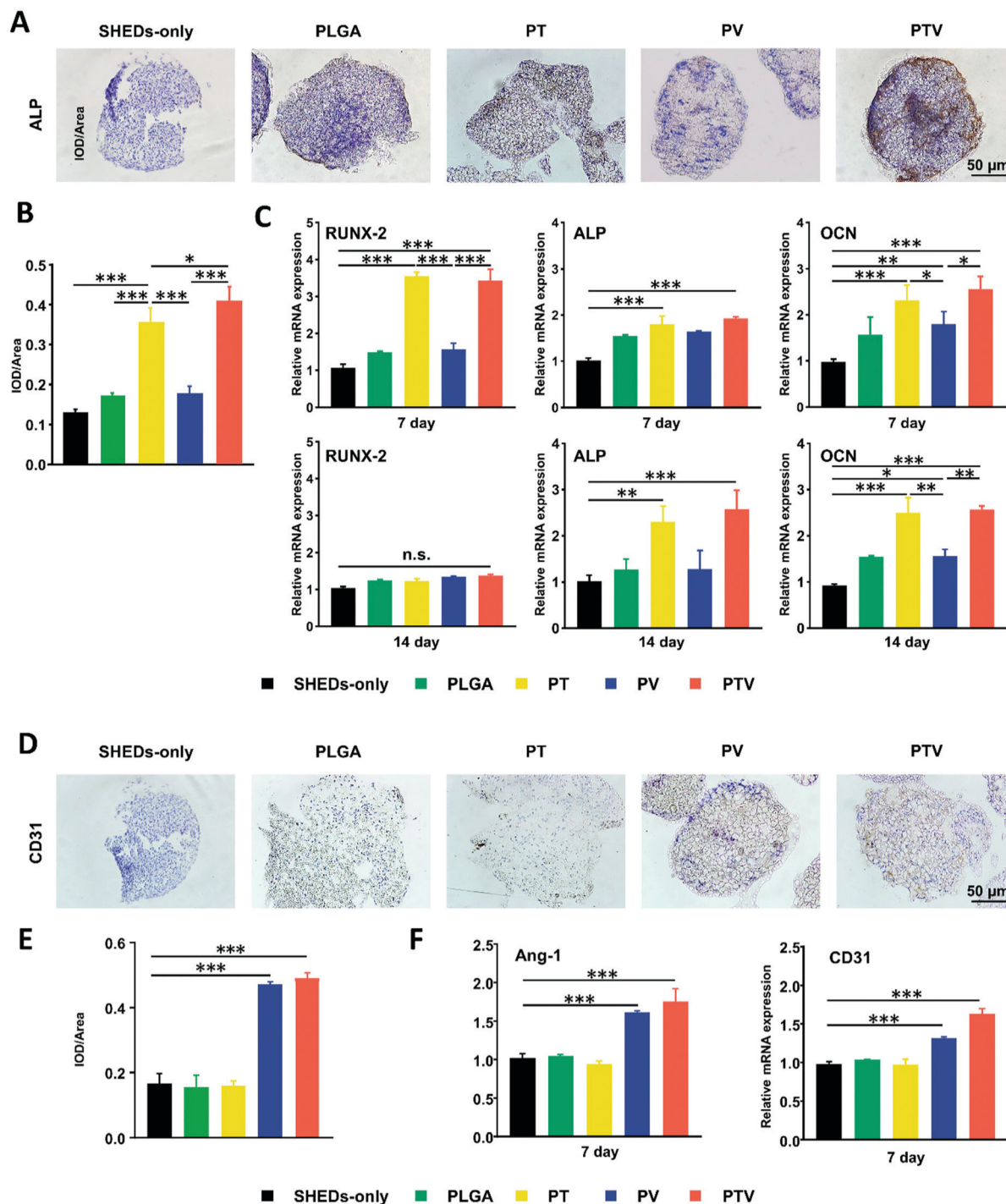


Fig. 6 Osteogenesis and angiogenesis function of microparticle-integrated aggregates. (A and B) IHC staining and quantitative analysis of ALP of SHED aggregates after 7 days of osteogenic induction. The relative expressions of two genes related to angiogenic differentiation were analyzed (C). (D and E) IHC staining and quantitative analysis of CD31 for SHED aggregates after 7 days of osteogenic induction. The relative expressions of three genes related to angiogenic differentiation were analyzed (F) (* $p < 0.05$, ** $p < 0.01$, *** $p < 0.001$).

showing few signs of bone formation. For the PTV groups, however, the defect areas were filled with a large amount of collagen-rich extracellular matrix, which had integrated with the surrounding host tissues. Masson trichrome staining revealed that the PTV groups showed more blue-stained areas, indicating immature collagen fibers (indicated by red arrows)

and osteoid, while the blank and PLGA groups showed mainly fibrous tissue. In particular, the PTV groups demonstrated much more newly formed blood vessels (indicated by blue arrows) at the defect site compared with the non-functional aggregates (PLGA group) and the blank group within 4 weeks. The immunohistochemical staining was carried out to evaluate

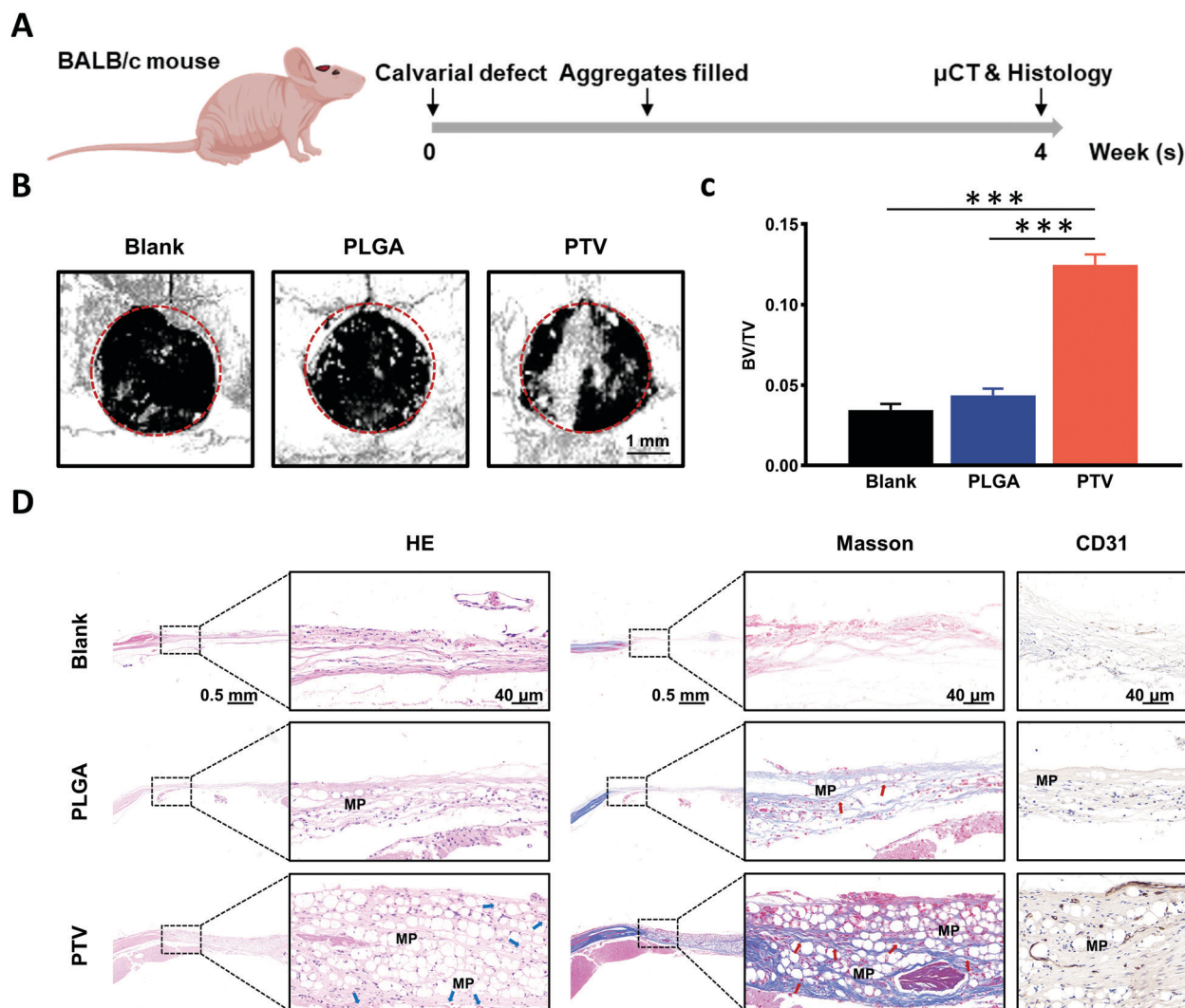


Fig. 7 Osteogenesis and angiogenesis effects of PTV/SHED aggregates *in vivo*. (A) Schematic illustration showing the design of the *in vivo* study. (B) Reconstructive 3D micro-CT photographs of repaired cranial bone defects in all groups at 4 weeks post-operation in nude mice (scale bar, 1 mm). (C) Quantitative analysis of BV/TV values for the three groups (* $p < 0.05$, ** $p < 0.01$, *** $p < 0.001$). (D) Histological analysis via H&E staining, Masson's trichrome staining and CD31 immunostaining of blank, PLGA and PTV groups after implantation at 4 weeks (at 4 \times and at 40 \times). MP represents the remnant microparticles; blue arrows indicate neo-vessel tissue; red arrows indicate collagen fiber connective tissue.

the expression of vascular endothelial cell marker (CD31). We found that a greater CD31-positive area was detected in the multifunctional (PTV) group compared with the other groups, which was consistent with the results in H&E staining. These results demonstrated that the aggregates with a specific differentiation ability showed significant potential for vascularized bone regeneration. However, further in-depth investigations with larger animals and long-term implantation will be required to fully understand the effect of multifunctional aggregates.

Conclusion

In summary, we designed a type of multifunctional aggregate fabricated through the co-culturing of SHEDs and hVE-cad-Fc-modified PLGA/ β -TCP microparticles. The integration of composite microparticles optimized the structure of the cell

aggregates, and thus significantly promoted the viability of the aggregates. Meanwhile, the composite aggregates (PTV/SHED aggregates) showed enhanced osteogenesis and angiogenesis *ex vivo*, which was attributed to the embedded β -TCP and surface-modified hVE-cad-Fc. The 3 mm calvarial defect model in mice suggested that PTV/SHED aggregates had promising potential in enhancing constructive vascularized bone remodelling *in vivo*. Taken together, the multifunctional aggregate could be an optimized platform for critical sized bone defect regeneration or used as a medicine screening system for orthopaedic disorders in the field of regenerative medicine.

Author contributions

Y. Zhao, Q. Cai, and J. Huang provided the laboratory resources and funding, and supervised the project; L. Zhang performed

the experimental work and data analysis; Z. Wan wrote the manuscript and plotted the schemes; Z. Yuan, Y. Zhang and J. Yang revised and edited the manuscript.

Conflicts of interest

There are no conflicts to declare.

Acknowledgements

The authors are grateful for the β -TCP nanoparticles, which were given as a present by the Institute of Metal Research, Chinese Academy of Science. This work was financially supported by the National Natural Science Foundation of China (11972001, 11772004 and 51873013) and the Beijing Natural Science Foundation (7212135).

Notes and references

- M. Shafiq, O. Ali, S. B. Han and D. H. Kim, *Front. Cell Dev. Biol.*, 2021, **9**, 747398.
- M. A. Gionet Gonzales and J. K. Leach, *Biomed. Mater.*, 2018, **13**, 034109.
- A. I. Hoch, V. Mittal, D. Mitra, N. Vollmer, C. A. Zikry and J. K. Leach, *Biomaterials*, 2016, **74**, 178–187.
- K. C. Murphy, A. I. Hoch, J. N. Harvestine, D. Zhou and J. K. Leach, *Stem Cells Transl. Med.*, 2016, **5**, 1229–1237.
- N. C. Cheng, S. Wang and T. H. Young, *Biomaterials*, 2012, **33**, 1748–1758.
- J. C. Valdoz, B. C. Johnson, D. J. Jacobs, N. A. Franks, E. L. Dodson, C. Sanders, C. G. Cribbs and P. M. Van Ry, *Int. J. Mol. Sci.*, 2021, **22**(23), 12690.
- S. B. Shah and A. Singh, *Acta Biomater.*, 2017, **53**, 29–45.
- J. I. Sasaki, G. L. Abe, A. Li, T. Matsumoto and S. Imazato, *Sci. Technol. Adv. Mater.*, 2021, **22**, 571–582.
- H. G. Augustin and G. Y. Koh, *Science*, 2017, **357**(6353), eaal2379.
- E. Gómez Barrena, P. Rosset, D. Lozano, J. Stanovici, C. Ermthaller and F. Gerbhard, *Bone*, 2015, **70**, 93–101.
- J. Filipowska, K. A. Tomaszewski, J. A. Walocha and T. Niedźwiedzki, *Angiogenesis*, 2017, **20**, 291–302.
- K. Hu and B. R. Olsen, *Bone*, 2016, **91**, 30–38.
- P. Chandra and A. Atala, *Clin. Sci.*, 2019, **133**, 1115–1135.
- K. Xu, Q. Shuai, X. Li, Y. Zhang, C. Gao, L. Cao, F. Hu, T. Akaike, J. X. Wang, Z. Gu and J. Yang, *Biomacromolecules*, 2016, **17**, 756–766.
- E. S. Harris and W. J. Nelson, *Curr. Opin. Cell Biol.*, 2010, **22**, 651–658.
- M. Giannotta, M. Trani and E. Dejana, *Dev. Cell*, 2013, **26**, 441–454.
- I. Paatero, L. Sauteur, M. Lee, A. K. Lagendijk, D. Heutschi, C. Wiesner, C. Guzmán, D. Bieli, B. M. Hogan, M. Affolter and H. G. Belting, *Nat. Commun.*, 2018, **9**, 3545.
- C. Gao, Y. Zhang, J. Xie, X. Wang, L. Cao, G. Chen, H. Mao, X. Bi, Z. Gu and J. Yang, *Appl. Mater. Today*, 2020, **20**, 100690.
- J. Xie, X. Li, Y. Zhang, T. Tang, G. Chen, H. Mao, Z. Gu and J. Yang, *J. Mater. Chem. B*, 2021, **9**, 3357–3370.
- Y. Petrenko, E. Syková and Š. Kubinová, *Stem Cell Res. Ther.*, 2017, **8**, 94.
- M. Yamada, A. Hori, S. Sugaya, Y. Yajima, R. Utoh, M. Yamato and M. Seki, *Lab Chip*, 2015, **15**, 3941–3951.
- K. Hayashi and Y. Tabata, *Acta Biomater.*, 2011, **7**, 2797–2803.
- Y. Kim, P. Baipaywad, Y. Jeong and H. Park, *Int. J. Biol. Macromol.*, 2018, **110**, 472–478.
- S. Hinkelmann, A. H. Springwald, A. Starke, H. Kalwa, C. Wölk, M. C. Hacker and M. Schulz Siegmund, *Mater. Today Bio*, 2022, **13**, 100190.
- K. Weibenbruch, E. D. Lemma, M. Hippler and M. Bastmeyer, *Curr. Opin. Biotechnol.*, 2021, **73**, 290–299.
- L. Cao, Y. Zhang, M. Qian, X. Wang, Q. Shuai, C. Gao, R. Lang and J. Yang, *Acta Biomater.*, 2019, **95**, 382–394.
- P. Xia, S. Wang, Z. Qi, W. Zhang and Y. Sun, *Artif. Cells, Nanomed., Biotechnol.*, 2019, **47**, 1662–1673.
- A. Nagai, T. Hattori, M. Hirose, A. Ogura, K. Nozaki, M. Aizawa and K. Yamashita, *Mater. Sci. Eng., C*, 2014, **34**, 214–220.
- Y. Wang, X. Yu, C. Baker, W. L. Murphy and T. C. McDevitt, *Acta Biomater.*, 2016, **29**, 42–51.
- N. Ramesh, S. C. Moratti and G. J. Dias, *J. Biomed. Mater. Res., Part B*, 2018, **106**, 2046–2057.
- R. Pampuch, *An Introduction to Ceramics*, 2014.
- M. Bohner, B. L. G. Santoni and N. Döbelin, *Acta Biomater.*, 2020, **113**, 23–41.
- H. S. Ching, N. Luddin, I. A. Rahman and K. T. Ponnuraj, *Curr. Stem Cell Res. Ther.*, 2017, **12**, 71–79.
- H. Wang, Q. Zhong, T. Yang, Y. Qi, M. Fu, X. Yang, L. Qiao, Q. Ling, S. Liu and Y. Zhao, *Mol. Med. Rep.*, 2018, **17**, 6551–6559.
- R. L. Carpenedo, S. A. Seaman and T. C. McDevitt, *J. Biomed. Mater. Res., Part A*, 2010, **94**, 466–475.
- L. Ferreira, T. Squier, H. Park, H. Choe, D. S. Kohane and R. Langer, *Adv. Mater.*, 2008, **20**, 2285–2291.
- C. C. Ahrens, Z. Dong and W. Li, *Acta Biomater.*, 2017, **62**, 64–81.
- R. L. Carpenedo, A. M. Bratt Leal, R. A. Marklein, S. A. Seaman, N. J. Bowen, J. F. McDonald and T. C. McDevitt, *Biomaterials*, 2009, **30**, 2507–2515.
- A. M. BrattLeal, R. L. Carpenedo, M. D. Ungrin, P. W. Zandstra and T. C. McDevitt, *Biomaterials*, 2011, **32**, 48–56.
- M. Ge, Y. Sheng, S. Qi, L. Cao, Y. Zhang and J. Yang, *J. Mater. Chem. B*, 2020, **8**, 9921–9932.
- C. T. Tsao, C. H. Chang, Y. Y. Lin, M. F. Wu, J. L. Wang, J. L. Han and K. H. Hsieh, *Carbohydr. Res.*, 2010, **345**, 1774–1780.
- K. Xu, Q. Shuai, X. Li, Y. Zhang, C. Gao, L. Cao, F. Hu, T. Akaike, J. X. Wang, Z. Gu and J. Yang, *Biomacromolecules*, 2016, **17**, 756–766.
- M. Nagaoka, K. Si Tayeb, T. Akaike and S. A. Duncan, *BMC Dev. Biol.*, 2010, **10**, 60.

- 44 T. J. C. Harris and U. Tepass, *Nat. Rev. Mol. Cell Biol.*, 2010, **11**, 502–514.
- 45 M. Miura, S. Gronthos, M. Zhao, B. Lu, L. W. Fisher, P. G. Robey and S. Shi, *Proc. Natl. Acad. Sci. U. S. A.*, 2003, **100**, 5807.
- 46 K. Nakajima, R. Kunimatsu, K. Ando, T. Ando, Y. Hayashi, T. Kihara, T. Hiraki, Y. Tsuka, T. Abe, M. Kaku, H. Nikawa, T. Takata, K. Tanne and K. Tanimoto, *Biochem. Biophys. Res. Commun.*, 2018, **497**, 876–882.
- 47 Q. Shuai, L. Cao, Z. Qin, Y. Zhang, Z. Gu and J. Yang, *J. Mater. Chem. B*, 2020, **8**, 1699–1712.
- 48 J. Xie, X. Li, Y. Zhang, T. Tang, G. Chen, H. Mao, Z. Gu and J. Yang, *J. Mater. Chem. B*, 2021, **9**, 3357–3370.
- 49 S. J. Kim, E. M. Kim, M. Yamamoto, H. Park and H. Shin, *Adv. Healthcare Mater.*, 2020, **9**, 2000608.
- 50 N. H. Lee, O. Bayaraa, Z. Zechu and H. S. Kim, *BMB Rep.*, 2021, **54**, 356–367.
- 51 M. Pelleitier and S. Montplaisir, *Methods Achiev. Exp. Pathol.*, 1975, **7**, 149–166.
- 52 X. Zhang, J. Fan, C. S. Lee, S. Kim, C. Chen, T. Aghaloo and M. Lee, *Adv. Funct. Mater.*, 2020, **30**, 201909218.
- 53 H. Nakahara, H. Misawa, T. Hayashi, E. Kondo, T. Yuasa, Y. Kubota, M. Seita, H. Kawamoto, W. A. Hassan, R. A. Hassan, S. M. Javed, M. Tanaka, H. Endo, H. Noguchi, S. Matsumoto, K. Takata, Y. Tashiro, S. Nakaji, T. Ozaki and N. Kobayashi, *Transplantation*, 2009, **88**, 346–353.
- 54 Z. K. Cui, S. Kim, J. J. Baljon, B. M. Wu, T. Aghaloo and M. Lee, *Nat. Commun.*, 2019, **10**, 3523.
- 55 J. Fan, C. S. Lee, S. Kim, C. Chen, T. Aghaloo and M. Lee, *ACS Nano*, 2020, **14**, 11973–11984.